

# Comparison between calculations and measurements of the forward and lateral radiation outside the TPS LINAC shielding room

Yu-Chi Lin<sup>1</sup>, Ang-Yu Chen<sup>1</sup>, Chien-Rong Chen<sup>1</sup>, Chih-Ching Liu<sup>1</sup>, Rong-Jiun Sheu<sup>2\*</sup>

<sup>1</sup>National Synchrotron Radiation Research Center, Hsinchu 30076, Taiwan

<sup>2</sup>Institute of Nuclear Engineering and Science, National Tsing Hua University, Hsinchu 30013, Taiwan

\* E-mail: rjsheu@mx.nthu.edu.tw

## Abstract

Forward and lateral radiation outside the TPS LINAC room during a full power beam commissioning were measured and compared with Monte Carlo predictions. Several high-sensitivity radiation detectors were used in this study to identify possibly increases of radiation above background level. Response functions of three different neutron detectors to both neutrons and high-energy gamma rays were calculated using MCNPX with continuous-energy cross sections. Neutron and gamma-ray spectra at the locations of measurement were estimated by FLUKA simulations. By folding the calculated spectra with detector response functions, we found that the calculated results are generally consistent with the measurements. However, some slight difference may hide some faults resulting from the simulation processes and the experiment methods. This paper presents the features of these detectors and an in-depth discussion on the neutron detector responses in this experiment. Although high-energy neutrons ( $>10$  MeV) are negligible for electron accelerators in this energy range, photoneutrons caused by interactions of high-energy gamma rays with the detector itself could be a significant contribution to the total response, especially when using a metal-embedded neutron detector at an environment with high-energy gamma rays.

## 1. Introduction

The TPS LINAC is essentially concatenated by three consecutive sections of linear accelerators with a nominal output of 2.25 W (150 MeV, 5 nC, 3 Hz) electron beam [1]. A 15 m long transfer line is used to guide the accelerated electrons from the LINAC outlet to the beam dump. The transfer line consists of four quadrupoles and a dipole magnet arranging in an order of Q1, Q2, Q3, D1, and Q4 along the beam trajectory. A dedicated beam dump made of iron core surrounded with lead and polyethylene was installed at the end of the transfer line to stop the beam. All of these components were installation at a simple rectangular shielding room made of 1 m thick concrete as a temporary laboratory named as LINAC LAB (Figure 1). To ensure radiation safety of personnel around the area, gamma-ray and neutron dose rates outside the LINAC room were repeatedly measured and reviewed during the commissioning.

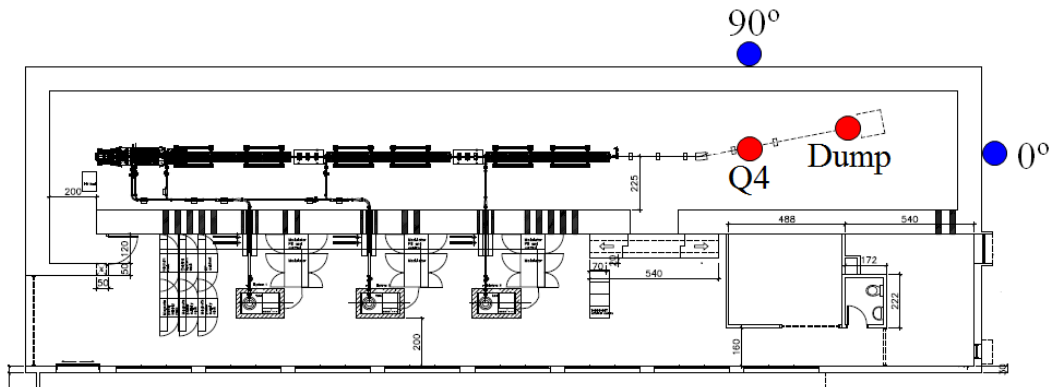


Figure 1. Layout of the LINAC LAB showing two possible beam loss points at Q4 and the beam dump (red spots), as well as the location of measurement (blue spot).

## 2. Materials and methods

### 2.1 LINAC radiation survey & radiation field calculations

Gamma-ray and neutron dose rates around the test area were constantly monitored from the start of LINAC commissioning. High dose rates up to several  $\text{mSv h}^{-1}$  outside the shielding room have been recorded during the initial mis-steering testing period. To identify similar situations from happening, frequent and comprehensive radiation survey is necessary especially for testing new lattice configuration. In addition to two area monitors installed at downstream and in a lateral direction, respectively, routine survey around the whole area was conducted by using VICTOREEN Model 451P ion chamber for measuring gamma-ray dose rates.

To explore the relationship between beam losses and dose distributions, the FLUKA code [1,2] was used to estimate gamma-ray and neutron dose rates around the LINAC LAB based on a series of simple beam loss scenarios. A rather detailed geometry model including main components of the accelerator, the bunker structure and local shielding was built aiming to predict useful dose rate maps practically. Beam loss estimation along the particle trajectory is difficult but crucial for an accurate dose evaluation of accelerators. Due to lack of reliable beam loss information for the LINAC operation, a series of point beam loss scenarios were assumed for dose distribution calculations. Following the direction of electron trajectory, beam loss locations were assigned at the LINAC outlet, Q1, Q2, Q3, D1, Q4, and the beam dump respectively.

## 2.2 Gamma and neutron detectors & response functions calculations

If all the accelerated electrons were perfectly dumped, dose rates outside the shielding room should be as low as comparable to the natural background. For monitoring gamma rays from the LINAC operation, we used a High Pressure Ionization Chamber (HPIC) model RSS-131-ER from GE Reuter-Stokes, which is designed to measure low-level gamma-ray radiation and capable of quick identifying small increases above background level. He-3 proportional counter model RS-P4-0818-202 from GE Reuter-Stokes was selected as the neutron probe. It is a cylindrical tube with an active volume of 2.54 cm in diameter and 45.72 cm in length and filled with 4 atm pure helium-3. Its sensitivity to thermal neutrons is about 54 counts per second per unit neutron flux (cps/nv). Three different detector configurations were assembled for monitoring neutrons from the LINAC operation. The first one is just the bare He-3 proportional counter; the second one uses the same type of neutron probe in the center and surrounded by 6.5 cm thick polyethylene to increase the detection efficiency for fast neutrons and to maximize the neutron counting for natural background; the third one is basically the same as the second detector, except that a layer of cylindrical polyethylene from the radius of 3.3 to the radius of 3.8 cm is replaced by lead to increase its sensitivity to high-energy neutrons. The three neutron detectors are denoted respectively as “Bare”, “PE”, and “PE+Pb” in the following sections. **Figure 2** shows a photo of these three self-assembled high-sensitivity neutron detectors and a HPIC for measuring gamma-ray dose rates.

Knowing the response function of a detector is essential for a meaningful application in radiation measurement. For the three self-assembled neutron detectors, we utilized MCNPX [3] with the LA150 neutron cross-section library to calculate their response functions because it has continuous-energy neutron cross sections up to 150 MeV. Full details of the neutron probe and moderator design were included in the calculation model. The integral response function of the PE detector was tested and verified in a standard neutron calibration room.

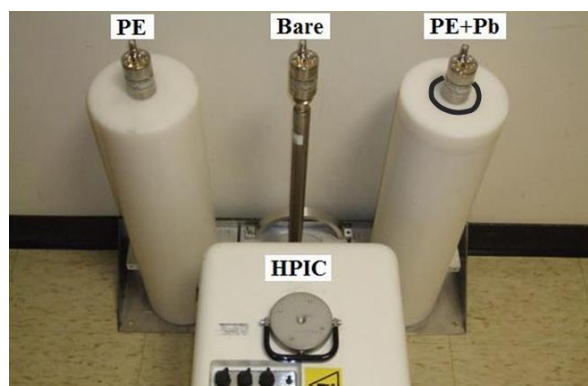


Figure 2. Three moderated-type neutron detectors denoted as Bare, PE, and PE+Pb, and a high-pressure ion chamber (HPIC) for gamma-ray dose rate measurements.

### 3. Results and Discussion

#### 3.1 Beam loss patterns and dose distributions

Different beam loss assumptions may lead to completely different dose distributions. A series of beam loss scenarios with different electron loss locations along the transfer line has been systematically studied by FLUKA simulations. The calculated results confirm the intuitive thoughts and provide quantitative estimates of the relationships. **Figure 3** shows a good example, where two gamma-ray dose rate distributions are obtained by simulating the primary electrons lost at three locations, respectively: (a) near the Q4 magnet and (b) the beam dump. **Figure 3** (left) presents top view of dose rate distributions and **Figure 3** (right) shows the corresponding dose distributions on the outside surface of the downstream shielding wall where the dose rates are usually the highest during the LINAC operation.

Differences between the resultant dose distributions caused by these two point beam loss scenarios are evident. It is therefore possible to take advantage of these distinguishing dose patterns in analyzing radiation survey data and their implications. This kind of information is very helpful in beam loss analysis for accelerator operation. For example, in case (b), if all the accelerated electrons are perfectly dumped as designed, gamma-ray dose rates outside the shielding should be quite low, comparable to a natural background level. Obviously, this was not what we have encountered during the LINAC commissioning. On the other hand, cases (a) in **Figure 3** show that a small amount of electrons lost at the transfer line will possibly cause significant dose rates somewhere outside the downstream shielding wall. Note that their projected dose patterns on the wall are different: case (a) shows a projected T-shaped shadow that reflects a rectangular lead local shielding and concrete supporting.

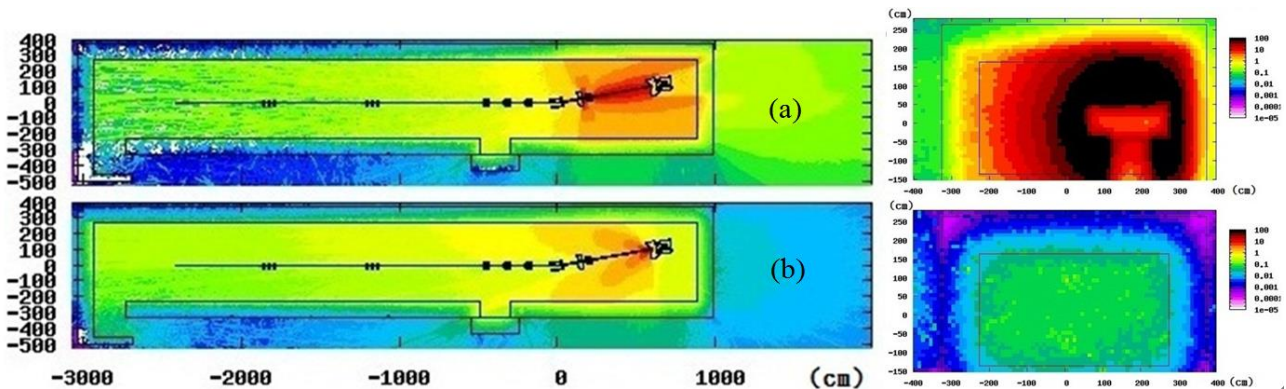


Figure 3. Gamma-ray dose rate ( $\mu\text{Sv h}^{-1} \text{W}^{-1}$ ) distributions around the LINAC area calculated for two beam loss scenarios: (a) electrons lost near the 4<sup>th</sup> quadrupole and (b) electrons lost at the beam dump.

#### 3.2 Comparison of calculations and survey

The dose distributions in **Figure 3** could be regarded as dose distribution profile to various beam loss scenarios since they are obtained based on a series of simple point-loss models. To demonstrate the usefulness and applications of these response functions, we analyzed a set of measurement data taken on September 23, 2011. Gamma-ray dose rates were measured at nine positions on the outer surface of the downstream concrete wall during a full-power operation. The measured dose rates are listed in Table 1 and their respective positions of measurement on the wall are illustrated in Figure 4. The labels P11-P33 mark the positions of measurement on the wall.

During the measurement, fluctuations in detector readings were in a range of about 10-30% because of several uncertainties and constraints, such as time limitation, detector sensitivity, and possible variation of machine operation. Even though the quality of the measured data may not be good, some valuable information could still be obtained from the dose distribution profile shown in **Figure 3**. As indicated by electron monitors mounted on the transfer line, approximately more than 95% of the accelerated electrons were successfully dumped into their destination. The beam dump has been designed to contain a full-power electromagnetic shower and to effectively attenuate secondary radiation by using lead and polyethylene. However, measured dose rates were found to be much higher than we previously predicted which is [4]

based on the assumption that all the electrons were attenuated inside the beam dump. Therefore we reasonably suspect that there must be a small portion of beam lost somewhere along the transfer line and causes the unexpected dose rates.

Examining the magnitude and pattern of measured dose rates (**Table 1**) as well as the calculated dose distribution profile, we realized that the number of electrons lost at Q4 will dominate the radiation field outside the downstream shielding wall. For simplify, we assumed all the accelerated electrons will either reach the beam dump or be lost by hitting the beam pipe near Q4. In **Table 1**, three similar beam loss scenarios are considered: (i) 1% beam lost at Q4 and 99% beam lost at the beam dump, (ii) 2% beam lost at Q4 and 98% beam lost at the beam dump, and (iii) 3% beam lost at Q4 and 97% beam lost at the beam dump. For case (i), the estimated dose rates on the wall are consistently lower than the measurement in most positions. On the other hand, case (iii) seems a little high compared with the measurement. To the best of our knowledge, the assumption of case (ii) appears to be the most likely scenario for the LINAC operation on September 23, 2011. The overall agreement between the estimated and measured dose rates is satisfactory considering the quality of the measured data and other uncertainties involved in the analysis.

Table 1. Comparison of calculated gamma-ray dose rates ( $\mu\text{Sv h}^{-1}$ ) and the measurement\* (September 23, 2011). The measurement uncertainties are estimated to be  $\sim 20\%$ .

Position	P11	P12	P13	P21	P22	P23	P31	P32	P33
Measured	2.7	5.3	4.2	2.7	8.3	7.3	11.9	0.3	8.8
1% at Q4	1.8 $\pm$ 1.0%	2.3 $\pm$ 3.6%	1.6 $\pm$ 3.6%	4.1 $\pm$ 2.0%	3.7 $\pm$ 2.0%	2.8 $\pm$ 2.7%	5.1 $\pm$ 2.1%	0.3 $\pm$ 4.6%	4.1 $\pm$ 3.2%
2% at Q4	3.6 $\pm$ 0.9%	4.5 $\pm$ 3.7%	3.2 $\pm$ 3.7%	8.0 $\pm$ 2.0%	7.3 $\pm$ 2.0%	5.5 $\pm$ 2.8%	10.2 $\pm$ 2.1%	0.5 $\pm$ 5.2%	8.2 $\pm$ 3.2%
3% at Q4	5.3 $\pm$ 0.9%	6.7 $\pm$ 3.7%	4.7 $\pm$ 3.7%	12.0 $\pm$ 2.0%	11.0 $\pm$ 2.0%	8.2 $\pm$ 2.8%	15.2 $\pm$ 2.1%	0.7 $\pm$ 5.4%	12.2 $\pm$ 3.2%

\* The operating conditions of LINAC were kept constant at about 5 nC, 3Hz, and 150 MeV during the measurement.

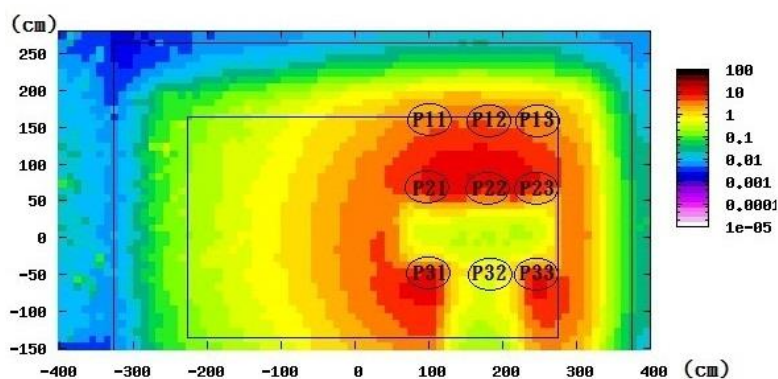


Figure 4. Gamma-ray dose rate ( $\mu\text{Sv h}^{-1}$ ) distribution on the outside surface of the downstream shielding wall calculated for an assumed beam loss scenario (2%Q4+98%Dump).

### 3.3 Response functions of neutron detectors

**Figure 5** (left) shows the MCNPX-calculated responses of three self-assembled neutron detectors (Bare, PE, and PE+Pb) to neutrons with various energies. Apparently, the bare detector is only sensitive to thermal neutrons. Surrounding by a 6.5 cm thick polyethylene as the neutron moderator, the PE detector is optimized for detecting neutrons in MeV range. The PE+Pb detector with a layer of lead embedded in the moderator, which is intended to increase the sensitivity of high-energy neutrons ( $\geq 10$  MeV) through (n,2n) reactions in lead. To validate our MCNPX calculation model, we have conducted an irradiation experiment of the PE detector in a standard neutron calibration room using a well-defined Cf-252 source. The calculated counting rate agrees well with the measurement and their difference is less than 2.5%. Also, the ambient dose equivalent conversion factor of the detector was determined to be  $0.0323 \mu\text{Sv h}^{-1}$  per cps.

Not only neutrons but also high-energy photons could cause counts to be registered by the neutron detectors. Bremsstrahlung photons, which usually dominate the radiation field in an electron accelerator, have a continuous energy distribution up to the primary electron energy. High-energy gamma rays may contribute to a neutron detector through an emission of photoneutrons, especially for a detector with high-Z materials in

its composition. The threshold energies of dominant photonuclear reactions are about 5-10 MeV for high-Z materials and the thresholds become much higher for low-Z materials [5]. Responses of these three neutron detectors to high-energy gamma rays were evaluated using MCNPX and the results are shown in **Figure 5** (right). Starting from 5-8 MeV, gamma rays contribute to the detector responses, especially for the extended neutron detector (PE+Pb) due to the relatively low threshold and high photonuclear cross sections of lead. Although the absolute magnitude of this gamma-ray response function is much lower than those neutron response functions, it is possible to have a substantial contribution to the detector if there were intense high-energy gamma rays in the area of interest.

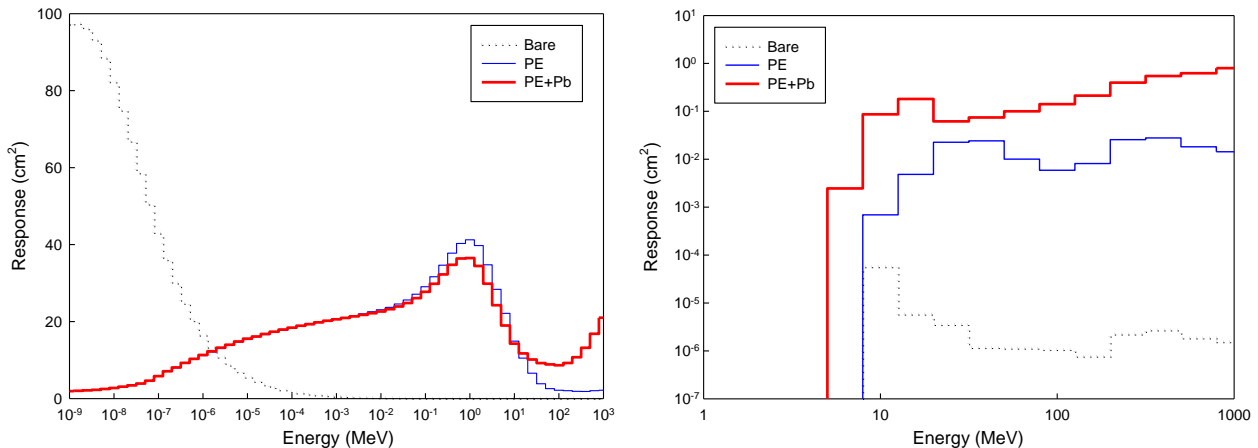


Figure 5. Response functions of three neutron detectors (denoted as Bare, PE, PE+Pb) to neutrons (left) and gamma rays (right) with various energies.

### 3.4 Radiation field simulation

Three neutron detectors were tested at both the forward and lateral positions of the TPS LINAC shielding room. Accurate beam loss assumption is the key for performing a practical accurate radiation field simulation. According to beam diagnosis information and our previous study on beam loss scenarios for the LINAC operation in section 3.2, there are two most probable beam loss locations: one is the design destination of all electrons, i.e. the beam dump, and the other is at the transfer line near the quadruple Q4. **Figures 6** and **Figures 7** show the resultant neutron and gamma-ray spectra scored at the two measurement locations for assuming 100% beam lost at the two locations, respectively. A comparison of neutron and gamma-ray spectra in **Figure 6** and **Figure 7** reveals several important characteristics of the radiation field. First, the neutron flux is much lower than that of gamma rays in both cases, in particular for the **Figure 6** second scenario assuming beam lost at Q4. Note that a multiplication factor of 1000 is applied in **Figure 6** for the neutron spectrum to fit in the same scale. In addition, the location of beam loss significantly affects the overall intensities and energy distributions of neutrons and gamma rays at the location of interest. Although more than 95% of the accelerated electrons are actually lost at the beam dump, these electrons are not important in terms of dose rates outside the shielding because of its nature of conservative design. In contrast, a small portion of the beam lost along the transfer line may cause significant gamma-ray or neutron dose rates at the forward and lateral directions. The energies of most gamma rays are between 0.1 and 10 MeV and most neutrons are in thermal range for electrons lost at the beam dump. In **Figure 6**, for electrons lost at Q4, the resultant spectra are somewhat different and have important implications for detector responses. Number of neutrons in MeV range is roughly comparable to that of thermal neutrons. High-energy neutrons ( $\geq 10$  MeV) are relatively minor in intensity. It is worth noting that there is an obvious high-energy tail ( $\geq 10$  MeV) in the gamma-ray spectrum of **Figure 6**. Those high-energy gamma rays may induce photonuclear reactions in particular when they interact with high-Z materials. Although the interaction probabilities of photonuclear reactions are probably lower than that of photoatomic reactions by a factor of 100 or more, number of photoneutrons and their contribution to a neutron detector could be important due to copious gamma rays existed in the radiation field. In **Figure 7**, rare high energy gamma ray above 10 MeV can induce photonuclear reactions in both cases. So less photonuclear reactions will happen when gamma rays interact with high-Z materials.

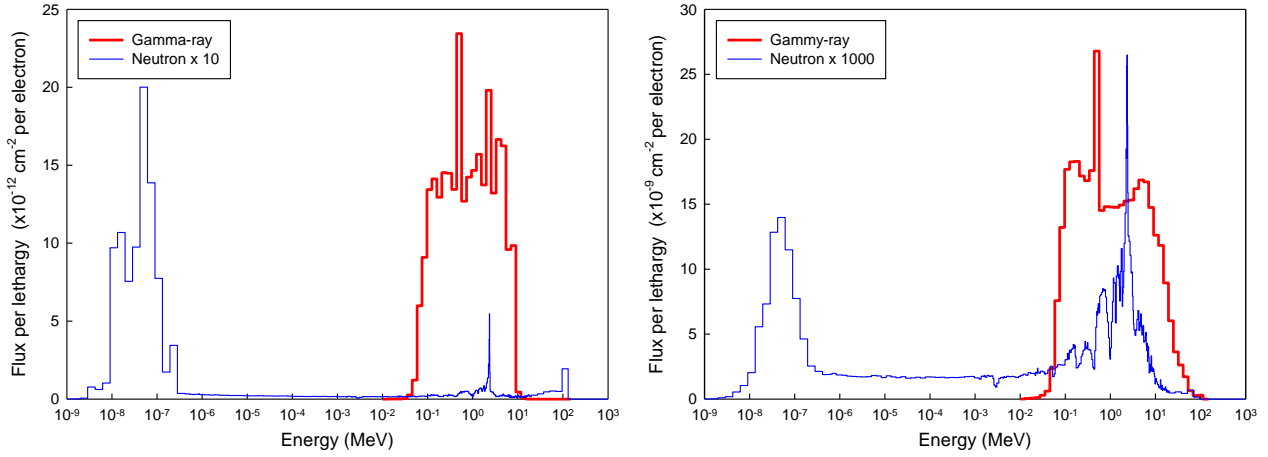


Figure 6. Neutron and gamma-ray energy spectra at the measurement location (forward direction) calculated for electrons lost at the beam dump (left) and near the 4<sup>th</sup> quadruple (right).

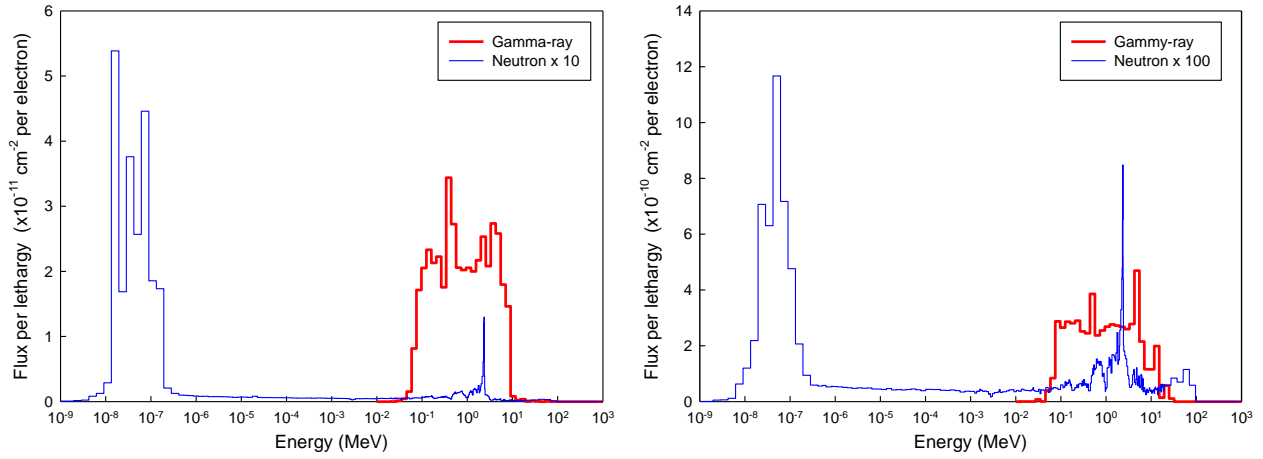


Figure 7. Neutron and gamma-ray energy spectra at the measurement location (lateral direction) calculated for electrons lost at the beam dump (left) and near the beam dump (right).

### 3.5 Measurements and data analysis

Three high-sensitivity neutron detectors (Bare, PE, and PE+Pb) and a high-pressure ionization chamber (HPIC) were used to measure neutron and gamma rays outside the downstream shielding wall during a full-power beam testing. The measured counting rates of three neutron detectors, gamma rays dose rates and neutron dose rate from the PE detectors are listed in **Table 2** and **Table 3**. In **Table 2**, the measured counting rate of the PE+Pb neutron detector is almost twice that of the PE detector, and we didn't expect so many high-energy neutrons for the operation of a 150-MeV electron accelerator. In order to examine the details of the radiation field, we have compared the measured results with a series of calculated detector responses, which were obtained by folding the detector response functions with the FLUKA predicted neutron and gamma-ray spectra at the location of measurement resulting from various beam loss scenarios. For example, **Table 2** and **Table 3** also lists three sets of calculated detector responses for 100% beam lost at the beam dump, 100% beam lost at Q4, and a combined scenario of 98% lost at the beam dump and 2% lost at Q4, respectively. Although most of the accelerated electrons are indeed successfully sent into the beam dump, our previous study indicated that a small portion of electrons lost near Q4 play a dominant role in the magnitude of downstream radiation. The assumption of 2% beam lost at Q4 and 98% beam lost at the beam dump was the most likely scenario for the LINAC operation during that time. Except for the bare neutron detector, the overall agreement between the estimated detector responses and measured results in **Table 2** is generally satisfactory considering many uncertainties in calculation assumptions and accelerator operation conditions. However, in **Table 3**, substantial differences exist between measured and calculational results. Measured counts are 10 times less than calculational results about. The discrepancy is likely that we simplify the calculation model too much, and we will review the detailed configuration of the beam dump. The

intensity of neutron dose at lateral side is around the background level and it is much smaller than forward direction intrinsically. We have duplicated the measurements and refined our simulation models, but it is difficult to reach good agreement between measurement and calculation in lateral case. Moreover, dead time and pile up phenomenon should be carefully evaluated when further measurements and studies are planned.

Another interesting observation is the significant contribution of photoneutrons to the PE+Pb detector. The detector was originally designed to increase the detection efficiency of high-energy neutrons. However, according to the calculated neutron spectra in **Figures 6**, neutrons with energies higher than 10 MeV only amount to a minor portion of the total neutrons at measurement location. In contrast, photoneutrons induced by high-energy gamma rays indeed contribute neutron counts to the PE+Pb detector by a large share. Folding the calculated gamma-ray spectrum at the measurement location with the detector response functions in **Figure 5**, we can estimate the photoneutron contribution to each of the three neutron detectors. As summarized in **Table 4**, photoneutrons do not have any contribution to the response of the bare detector but account for about 3.7% of neutron counts registered by the PE detector. The most surprising result is for the PE+Pb detector, in which approximately 38% of neutron counts are coming from photoneutrons. The counting rate ratio of the PE+Pb detector to the PE detector could be originally regarded as an indicator of high-energy neutron significance in a specific radiation field. Here, it is however related to high-energy gamma rays. The higher the ratio, the more counts registered by the detector are resulting from photoneutrons originated from the detector itself. In this study, the measured ratio is 1.86 (536.2/287.7) while the calculated ratio is 1.51 (482.8/320.7). This number indicates that there are plenty high-energy gamma rays in the radiation field and the photoneutron contribution to the detector response should be carefully evaluated. It also suggests that using an extended range neutron detector in an environment with high-energy gamma rays may overestimate the ambient neutron dose rates.

Table 2. Comparison of measured neutron counting rates (counts per minute), neutron and gamma-ray dose rates in forward direction ( $\mu\text{Sv h}^{-1}$ ) with the calculated results.

LINAC (2.25W)	Meas.	Calc. (100%DP)	Calc. (100%Q4)	Calc. (98%DP+2%Q4)
Bare (cpm)	386.4±5.4%	1112.4±18.7%	8995.2±5.4%	1270.0±16.0%
PE (cpm)	287.7±12.75%	141.1±8.2%	9123.1±0.6%	320.7±3.6%
PE+Pb (cpm)	536.2±4.5%	142.8±8.5%	17146.4±2.3%	482.8±3.0%
Neutron ( $\mu\text{Sv/h}$ )	0.15±12.75%	0.05±28.1%	3.80±1.9%	0.13±11.3%
Gamma-ray ( $\mu\text{Sv/h}$ )	6.38±1.7%	0.12±3.4%	172.05±2.4%	3.56±2.3%

Table 3. Comparison of measured neutron counting rates (counts per minute), neutron and gamma-ray dose rates in lateral direction ( $\mu\text{Sv h}^{-1}$ ) with the calculated results.

LINAC (2.25W)	Meas.	Calc. (100%DP)	Calc. (100%Q4)	Calc. (98%DP+2%Q4)
Bare (cpm)	57.6±17.6%	2796.2±23.6%	5473.1±11.9%	2849.7±22.7%
PE (cpm)	44.0±14.2%	377.8±9.62%	1943.2±2.5%	409.1±8.7%
PE+Pb (cpm)	55.8±12.0%	371.2±9.86%	1951.9±3.2%	402.8±8.9%
Neutron ( $\mu\text{Sv/h}$ )	0.02±14.2%	0.10±6.60%	0.89±7.4%	0.11±5.7%
Gamma-ray ( $\mu\text{Sv/h}$ )	0.35±1.9%	0.19±5.07%	2.57±13.3%	0.23±4.9%

Table 4. Ratio of neutron and photoneutron responses for three neutron detectors.

LINAC (2.25W)	Calc.	Neutrons	Photoneutro ns
Bare (cpm)	1270.0	100%	0.0%
PE (cpm)	320.7	96.3%	3.7%
PE+Pb (cpm)	482.8	61.6%	38.4%

#### 4. Conclusions

The pre-injector of the TPS is a 150-MeV electron LINAC with a nominal output of 2.25 W. The accelerated electrons are capable of producing intense secondary radiation and causing high dose rates outside the shielding if the electrons are not properly dumped and shielded. A series of FLUKA simulations on the dose

distribution was performed by assuming various point losses along the transfer line. Some resultant dose distributions are distinguishable with each other and can be regarded as dose distribution profile, which are useful in our beam loss diagnosis and analysis of measured dose rates. In the case of analysis, an assumption of 2% beam lost at Q4 and 98% beam lost at the beam dump is the most probably beam loss scenario judging from the magnitude and the pattern of measured gamma-ray dose rates.

Three high-sensitivity moderated-type neutron detectors were assembled, calibrated, and tested at the TPS LINAC. Detector response functions to neutrons and gamma rays with various energies were calculated by continuous-energy MCNPX calculations. Absolute neutron and gamma-ray spectra at the location of measurement were estimated by FLUKA simulations. Total counting rates of the detectors can be estimated by folding the resultant neutron and gamma-ray spectra with corresponding detector response functions. Based on the assumption of 2% beam lost at Q4 and 98% at the beam dump, the calculated results of the detector responses are mostly consistent with the measurements of forward direction outside the TPS LINAC shielding room. For neutron measurements outside the downstream shielding wall of the TPS LINAC, high-energy neutrons (>10 MeV) are negligible, but photoneutrons caused by interactions of high-energy gamma rays with the detector could be a significant factor in the total response, especially for an extended range neutron detector. For some reasons including more specific FLUKA model and considerations of dead time and pile up phenomenon, the experiment and simulation data have some different results so far. So before discussing more detail of those data, further studies are necessary to investigate, especially for those discrepancies results in lateral direction.

## References

- [1] NSRRC, *Taiwan Photon Source (TPS) design handbook*, National Synchrotron Radiation Research Center (2009).
- [2] A. Fasso`, A. Ferrari, J. Ranft, and P.R. Sala, *FLUKA: a multi-particle transport code*, CERN-2005-10, INFN/TC\_05/11, SLAC-R-773 (2005).
- [3] G. Battistoni, S. Muraro, P.R. Sala, F. Cerutti, A. Ferrari, S. Roesler, A. Fasso`, and J. Ranft, The FLUKA code: Description and benchmarking, *Proc. Hadronic Shower Simulation Workshop 2006*, Sep. 6-8, Fermilab (2006). M. Albrow and R. Raja Eds., AIP Conference Proceeding 896, 31-49 (2007).
- [4] D.B. Pelowitz (Ed), *MCNPX User's Manual, Version 2.7.0*, LA-CP-11-00438, Los Alamos National Laboratory (2011).
- [5] R.J. Sheu, J. Liu, J.P. Wang, K.K. Lin, and G.H. Luo, Characteristics of prompt radiation field and shielding design for Taiwan Photon Source, *Nucl. Technol.* 168 (2009), pp. 417-423.
- [6] W.P. Swanson, *Radiological safety aspects of the operation of electron linear accelerators*, IAEA Technical Reports Series No. 188, International Atomic Energy Agency (1979).